# EKF and UKF-Based Estimation of a Sensor-Less Axial Flux PM Machine under an Internal-Model Control Scheme using a SVPWM Inverter

Araz Darba[1], Karim Salahshoor[2]

1. Azad University of South Tehran Branch, Tehran, Iran E-mail: arazdarpa@yahoo.com

2. Petroleum University of Technology, Tehran, Iran E-mail: Salahshoor@put.ac.ir

**Abstract:** This paper presents a comparative estimation study of rotor speed and position of a sensor-less axial flux permanent magnet synchronous motor (AFPMSM) drive system using extended Kalman filter (EKF) and unscented Kalman filter (UKF) algorithms. An internal model control (IMC) strategy is introduced to control the AFPMSM drive through currents, leading to an extension of PI control with integrators added in the off-diagonal elements to remove the cross-coupling effects between the applied voltages and stator currents in a feed-forward manner. The reference voltage is applied through a space vector pulse width modulation (SVPWM) unit. A diverse set of test scenarios has been realized to comparatively evaluate the state estimation of the sensor-less AFPMSM drive performances under the implemented IMC-based control regime using a SVPWM inverter. The resulting MATLAB simulation outcomes in the face of no-load, nominal load and speed reversal clearly illustrate the well-behaved performances of the two estimation algorithms. The UKF seems to be more promising under noisy conditions. Nevertheless, there is no clear preference for either where steady-state performance is more critical.

**Key Words:** Sensor-less, AFPMSM, SVPWM, IMC, EKF, UKF

## 1 INTRODUCTION

In recent years, a great deal of interest has been dedicated to develop digital control techniques to industrial AC drive systems and variable speed drives. Space vector pulse-width modulation (SVPWM) presents one of the most efficient methods for this purpose which relies on analysis of three-phase inverter in the complex plane by the Space Vector theory. Compared to the conventional sinusoidal pulse width modulation (SPWM), SVPWM is more suitable for digital implementation and can increase the obtainable maximum output voltage with maximum line voltage. Moreover, it can obtain a better voltage total harmonic distortion factor. The SVPWM main goal is to achieve symmetrical 3-phase sine voltage waveforms of adjustable voltage and frequency, while SVPWM takes the inverter and motor as a whole, using the eight fundamental voltage vectors, to realize variable frequency of voltage and speed adjustment[1]-[5].

In the recent years, paramagnet magnet (PM) machines have gained more popularity than induction motors in some fields of AC variable speed drives due to the availability of new PM materials that can introduce more energy and field. These machines lack any windings in the rotors and hence do not produce rotor resistive loss, leading to more efficiency than induction motor drives.

PM machines are often classified in two groups: brushless DC (BLDC) and permanent magnet synchronous motor (PMSM). In BLDC machines, back-EMF is trapezoidal and hence they are prone to produce more harmonics and losses especially in high speeds in contrast to PMSM machines due to the sinusoidal back-EMF [6].

This work is supported by National Nature Science Foundation under Grant ×××××××

First electrical machines are Axial Flux and their excitation system was magnetic (M. Faraday 1831). In recent years Axial flux machines because of two significant features are more considered: high moment of inertia and low speed. Both of these properties are due to impact structure and high diagonal size. High moment of inertia plays the flywheel role and so rotor speed remains stable. And low speeds are available because of high diagonal size and rotor can hold more pole-pairs, this feature is more interesting in tensional and lifting application. And mechanical gear box is needed no more and this reduces cost and increases efficiency of system [7], [8].

## 2 STATE ESTIMATION OF A SENSOR-LESS MOTOR

Sensor-less strategies have been developed to overcome technical problems raised in the conventional drive systems. Back-EMF can be used to estimate rotor position and speed in high speeds. However, it is useless in low speeds and stand-still conditions because of the small induced voltage. Kalman filter (KF) can provide optimal estimations of rotor position and speed, based on a valid linear dynamic model of the motor, for both high and low speeds. Extended Kalman filter (EKF) presents an alternative estimation methodology once the motor can no longer be represented by a linear dynamic model. EKF needs to calculate a linear model of the system on the working operating point and this might be considered as a drawback for an observer or estimator because it is costly, complex and time consuming. UKF provides an alternative estimation tool for such highly non-linear applications which do not rely upon any linearization procedure. It uses a deterministic sampling approach to capture the state mean and covariance propagations with a minimal set of sampling points.

## 3 SENSOR-LESS AFPMSM DRIVE

The stator windings of an axial flux PM motor are different from its radial flux PMSM counterpart. The main difference lies in stator parameters which necessitate calculating inductances that is very low in these machines comparing radial flux machines. But, this is not needed in the former because these parameters can be obtained by measurements. As a consequence, we can use conventional PMSM model for the axial flux PMSM. In addition, there is no difference between the back-EMF produced by a permanent magnet with that produced by an excited coil [8]. Hence, the mathematical model of an axial flux permanent magnet synchronous motor is similar to that of the radial PMSM.

The following assumptions are made in the model derivation:

a) Saturation is neglected although it can be taken into account by parameter changes.

b) The back-EMF is sinusoidal.

c) Eddy currents and hysteresis and stray losses are negligible.

Accordingly, the stator d and q equations in the rotor reference frame are given by [6]:

$$v_d = Ri_d + p\lambda_d - \omega_s\lambda_q \quad (1)$$

$$v_q = Ri_q + p\lambda_q - \omega_s\lambda_d \quad (2)$$

Where

$$\lambda_q = L_q i_q \quad (3)$$

$$\lambda_d = L_d i_d + \lambda_{af} \quad (4)$$

$v_d$ and $v_q$ are the *d* and *q* axis voltages, $i_d$ and $i_q$ denote the *d* and *q* axis stator currents, $L_d$ and $L_q$ indicate the *d* and *q* axis inductances, $\lambda_d$ and $\lambda_q$ are the *d* and *q* axis stator flux linkages, while *R* and $\omega_s$ represent the stator resistance and inverter frequency, respectively. $\lambda_{af}$ is the flux linkage due to the rotor magnets linking the stator. The electric torque can be expressed by:

$$T_e = 3P\left[\lambda_{af} i_q + \left(L_d - L_q\right) i_d i_q\right]/2 \quad (5)$$

And the equation for motor dynamic is:

$$T_e = T_l + B\omega_r + JP\omega_r \quad (6)$$

*P* denotes the number of pole-pairs, $T_l$ indicates the load torque, *B* show the damping coefficient, $\omega_r$ is the rotor speed, and *J* is the moment of inertia.

The inverter frequency is related to the rotor speed as follows:

$$\omega_s = P\omega_r \quad (7)$$

The machine model is nonlinear as it contains product terms such as speed with $i_d$ and $i_q$.

For dynamic simulation, the equations of the PMSM, summarized in (1)-(6), must be expressed in the following state-space form:

$$P\omega_r = (T_e - T_l - B\omega_r)/J \quad (8)$$

$$Pi_d = \left(v_d - Ri_d + \omega_s L_q i_q\right)/L_d \quad (9)$$

$$Pi_q = \left(q - Ri_q - \omega_s L_d i_d - \omega_s\lambda_{af}\right)/L_q \quad (10)$$

The *d* and *q* variables are obtained from *a*, *b*, *c* variables through the Park transform, defined as:

$$\begin{bmatrix} v_d \\ v_q \\ v_o \end{bmatrix} = \begin{bmatrix} cos(\theta) & cos(\theta - 2\pi/3) & cos(\theta + 2\pi/3) \\ sin(\theta) & sin(\theta - 2\pi/3) & sin(\theta + 2\pi/3) \\ 1/2 & 1/2 & 1/2 \end{bmatrix} . \begin{bmatrix} v_a \\ v_b \\ v_c \end{bmatrix} \quad (11)$$

The *a*, *b*, *c* variables are obtained from the *d*, *q* variables through the inverse of the Park transform as follows:

$$\begin{bmatrix} v_a \\ v_b \\ v_c \end{bmatrix} = \begin{bmatrix} cos(\theta) & sin(\theta) & 1 \\ cos(\theta - 2\pi/3) & sin(\theta - 2\pi/3) & 1 \\ cos(\theta + 2\pi/3) & sin(\theta + 2\pi/3) & 1 \end{bmatrix} . \begin{bmatrix} v_d \\ v_q \\ v_o \end{bmatrix} \quad (12)$$

## 4 SVPWM INVERTER

Space vector modulation (SVM) represents one of the preferred real-time modulation technique which is widely employed for digital control of voltage source inverters [9], [10]. This section presents a concise introduction to the principle and implementation of the space vector modulation for a two-level inverter.

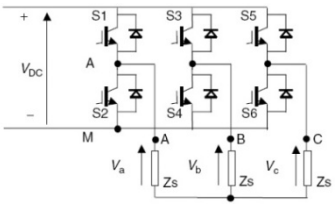


Fig. 1: Three phase, two level inverter

The operating status of the switches in the two-level inverter, shown in Fig. 1, can be represented by switching states. The switching state 'P' denotes that the upper switch in an inverter leg is on and the inverter terminal voltage ($V_{AN}, V_{BN}, V_{CN}$) is positive ($+V_{dc}$) while 'O' indicates that the inverter terminal voltage is zero due to the conduction of the lower switch. Therefore, there are eight possible combinations of switching states in the two-level inverter as listed in Table 1. The switching state [POO], for example, corresponds to the conduction of *S*1, *S*6, and *S*2 in the inverter legs *A*, *B*, and *C*, respectively. Among the eight switching states, [PPP] and [OOO] are zero states and the others are active states.

Tab. 1: Space Vectors, Switching States, On State Switches, Vector Definitions

| Space Vector | Switching States | On State Switches | Vector Definition |
|---|---|---|---|
| $\vec{V}_0$ | [PPP] [OOO] | $S_1, S_3, S_5$ $S_4, S_6, S_2$ | $\vec{V}_0 = 0$ |
| $\vec{V}_1$ | [POO] | $S_1, S_6, S_2$ | $\vec{V}_1 = \sqrt{2}\left(\sqrt{2}V_{dc} + \sqrt{3}V_\alpha + V_\beta\right)/4V_{dc}$ |
| $\vec{V}_2$ | [PPO] | $S_1, S_3, S_2$ | $\vec{V}_2 = \left(V_{dc} + \sqrt{6}V_\alpha\right)/2V_{dc}$ |
| $\vec{V}_3$ | [OPO] | $S_4, S_3, S_2$ | $\vec{V}_3 = \sqrt{2}\left(\sqrt{2}V_{dc} + \sqrt{3}V_\alpha - V_\beta\right)/4V_{dc}$ |
| $\vec{V}_4$ | [OPP] | $S_4, S_3, S_5$ | $\vec{V}_4 = \sqrt{2}\left(\sqrt{2}V_{dc} + \sqrt{3}V_\alpha + V_\beta\right)/4V_{dc}$ |
| $\vec{V}_5$ | [OOP] | $S_4, S_6, S_5$ | $\vec{V}_5 = \left(V_{dc} + \sqrt{6}V_\alpha\right)/2V_{dc}$ |
| $\vec{V}_6$ | [POP] | $S_1, S_6, S_5$ | $\vec{V}_6 = \sqrt{2}\left(\sqrt{2}V_{dc} + \sqrt{3}V_\alpha - V_\beta\right)/4V_{dc}$ |

The active and zero switching states can be represented by active and zero space vectors, respectively. A typical space vector diagram for the two-level inverter has been illustrated in Fig. 2, where the six active vectors $\vec{V}_1$ to $\vec{V}_6$ form a regular hexagon with six equal sectors (I to VI). The zero vector $\vec{V}_0$ lies on the center of the hexagon.

### 4.1 Simulation of SVPWM

Based on the principles of SVPWM, the simulation models for generating SVPWM waveforms mainly include the sector selection, gate switching time calculation, and generation of SVPWM waveforms. At the first, it is necessary to determine that the current voltage vector is within which sector.

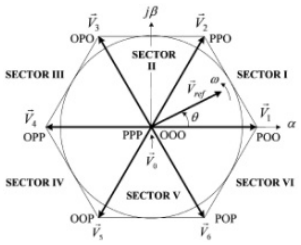


Fig. 2: Diagram of voltage space vector

Considering that the expression of vector in the $\alpha$-$\beta$ coordinate system is suitable for control implementation, the angle can be determined in a fuzzy manner from $\alpha$-$\beta$ form of voltage vector. For this purpose, atan2 function is utilized by the virtue of considering speed reversal action. The atan2 function provides angle in radians that must be converted to degree, the sector selection implemented in Tab. 2.

Tab. 2: Sector selection rule

| Angle | Sector |
|---|---|
| From 0 to 60 | 1 |
| From 60 to 120 | 2 |
| From 120 to 180 | 3 |
| From -180 to -120 | 4 |
| From -120 to -60 | 5 |
| From -60 to 0 | 6 |

In the next step, gate switching time is calculated. Gate on and off time is then calculated as follows:

$$T_{ON} = (1 - V)/2 \quad (13)$$

$$T_{OFF} = (1 + V)/2 \quad (14)$$

$V$ is the specified voltage vector from Table 1 according to the selected sector.

For generating logic gate command, a ramp signal is generated and then compared with gate switching times of each phase. Gate commands of inverter's switches are generated via Table 3.

Tab. 3: Gate Command Signal Generation

| Phase A | | Phase B | | Phase C | |
|---|---|---|---|---|---|
| If $T_{OFF} \le R \le T_{ON}$ | | If $T_{OFF} \le R \le T_{ON}$ | | If $T_{OFF} \le R \le T_{ON}$ | |
| Switch 1 ON | Switch 2 OFF | Switch 3 ON | Switch 4 OFF | Switch 5 ON | Switch 6 OFF |
| Else | | Else | | Else | |
| Switch 1 OFF | Switch 2 ON | Switch 3 OFF | Switch 4 ON | Switch 5 OFF | Switch 6 ON |

## 5 CURRENT CONTROLLER

### 5.1 Internal Model Control

In this paper, the internal model control (IMC) method [11] has been introduced and applied through current control scheme, as depicted in Fig. 3. The main benefits of the IMC methodology are the followings. It leads to synchronous frame PI-type current controllers. The controller parameters (i.e., gain and integration time) can be expressed directly in certain machine parameters and the desired closed-loop bandwidth. This simplifies the design procedure and hence trial-and-error steps are avoided.

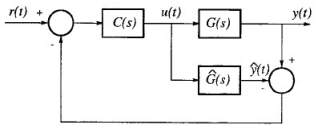


Fig. 3: IMC structure

IMC is considered as a *robust control* method [7]. Its structure uses an internal model $\hat{G}(s)$ in parallel with the controlled system $G(s)$. For an ac machine, output represents the stator voltage and current vectors, respectively, while $r = \begin{bmatrix} i_d^{ref} & i_q^{ref} \end{bmatrix}^T$ indicates the current set-point vector. The control loop is augmented by a block $C(s)$; the so-called *IMC controller*. $G(s)$, $\hat{G}(s)$ and $C(s)$ are all transfer function matrices.

### 5.2 Controller design for the axial flux PMSM

Since $G(s)$ has no right-half-plane zeros and behaves as a first-order system for high frequencies, it can be written:

$$G(s) = G^{-1}(s)L(s) \quad (15)$$

Where all diagonal elements may be selected equal as:

$$L(s) = (\alpha I)/(s + \alpha) \quad (16)$$

*The tuning problem, which for a PI controller involves adjustment of two parameters, is hence reduced to the selection of one parameter only, the desired closed-loop bandwidth*. Since, for a first-order system, the rise time $t_r$ is related to $\alpha$ as $t_r = \ln 9 / \alpha$, a specification of the $t_r$ immediately yields the desired bandwidth and, in turn, a suitable controller. The equivalent classic controller can be found as:

$$F(s) = \alpha \begin{bmatrix} L_d\left(1 + \frac{R_s}{sL_d}\right) & -\frac{\omega_r L_q}{s} \\ \frac{\omega_r L_q}{s} & L_q\left(1 + \frac{R_s}{sL_q}\right) \end{bmatrix} \quad (17)$$

$$F_{PI}(s) = \begin{bmatrix} K_d\left(1 + \frac{1}{sT_{id}}\right) & 0 \\ 0 & K_q\left(1 + \frac{1}{sT_{iq}}\right) \end{bmatrix} \quad (18)$$

It is, thus, more straightforward to implement the classic structure than the IMC structure, shown in Fig. 3. A comparison with two standard PI controllers (for the $d$ and $q$ loops) shows that (17) is an extension of PI control with integrators added in the anti-diagonal elements of $F(s)$ in order to remove the cross coupling effects, with:

$$K_d = \alpha L_d\,, K_q = \alpha L_q\,, T_{id} = \frac{L_d}{R_s}\,, T_{iq} = \frac{L_q}{R_s} \quad (19)$$

Figure 4 shows the schematic diagram of the current controller. Two PI controllers are employed to regulate the stator currents and feed-forward control is then used to decouple the dynamics between the applied voltages and the currents. The inputs of the current controller are the current reference and the rotor speed, while its output is the reference voltage. The reference voltage will be applied to

SVPWM unit. The outputs of the PI controllers are limited and have anti-reset windup. Compensation methods can be used to improve the performance at low speeds.

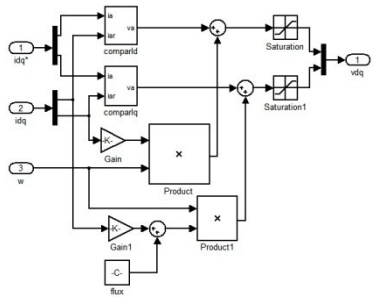


Fig. 4: Current controller block

# 6 STATE ESTIMATION

## 6.1 Motor nonlinear equations

To avoid convergence problems at startup and to simplify the motor equations, the rotor reference frame is chosen for evaluation of the Kalman filters [12]. The motor nonlinear state equations can be expressed in the form:

$$\begin{aligned} \dot{x}(t) &= F\big(x(t)\big)x(t) + Gu(t) \\ y(t) &= Hx(t) \end{aligned} \tag{20}$$

Where $u = [u_d \quad u_q]'$ and $y = [i_d \quad i_q]'$ are the input and the output vectors, respectively. The state variables are:

$$x = [i_d \quad i_q \quad \omega_e \quad \theta_e] \tag{21}$$

The system state matrices are defined as:

$$F\big(x(t)\big) = \begin{bmatrix} -\frac{R}{L_d} & \omega_e \frac{L_q}{L_d} & 0 & 0 \\ -\omega_e \frac{L_d}{L_q} & -\frac{R}{L_q} & -\frac{K_e}{L_q} & 0 \\ 0 & 0 & 0 & 0 \\ 0 & 0 & 1 & 0 \end{bmatrix} \tag{22}$$

$$G = \begin{bmatrix} \frac{1}{L_d} & 0 & 0 & 0 \\ 0 & \frac{1}{L_q} & 0 & 0 \end{bmatrix}^T, \qquad H = \begin{bmatrix} 1 & 0 & 0 & 0 \\ 0 & 1 & 0 & 0 \end{bmatrix}^T \tag{23}$$

## 6.2 EKF algorithm

The EKF is an optimal estimator in the least square sense for the estimation of nonlinear dynamic systems. It is derived from the Kalman filter based on successive linearization of the signal process and observation map [14]. More details can be found in a previous work [13]. For this application, the motor nonlinear state equations (20) are expressed in the discretized form:

$$x_{k+1} = F_d(x_k)x_k + G_d u_k + w_k \tag{24}$$

$$y_k = H_d x_k + v_k \tag{25}$$

The state model, represented by (24) and (25), also includes the statistical description for the inaccuracies, where $w_k = w(kT_s)$ and $v_k = v(kT_s)$ are, respectively, the zero mean Gaussian process and measurement noise vectors with covariance matrices $Q$ and $R$. The discretized matrices are derived using the exponential Taylor approximation [15]-[16], assuming a small sampling time and the use of zero-order-hold (ZOH) sampling technique.

$$F_d \cong I + FT_s\,,\; G_d = GT_s\,,\; H_d = H \tag{26}$$

The basic idea of the EKF is to linearize the state-space model represented by (24) and (25) at each time instant around the most recent state estimate, which is taken at $\hat{x}_k$ or $\hat{x}_{k-1}$. Once a linear model is obtained, the standard Kalman filter equations can be applied. The prediction of the state covariance requires the online computation of Jacobian matrix $\Phi$, defined as:

$$\Phi_{k-1} = \left.\frac{\partial F\big(x(t)\big)x(t)}{\partial x}\right|_{x=\hat{x}_{k|k-1}} = \left.\frac{\partial \dot{x}}{\partial x}\right|_{x=\hat{x}_{k|k-1}} \tag{27}$$

The Jacobian of $H$ is not calculated because $H$ is linear. The discretized Jacobian of $\Phi_{k-1}$ will be approximated as:

$$\Phi_{d,k-1} \cong I + \Phi_{k-1} T_s \tag{28}$$

For a given sampling time $t_k$, the optimal state estimation $\hat{x}_{k|k}$ and its covariance matrix $\hat{P}_{k|k}$ are generated by the filter through a two-step loop. The first step performs a prediction of both quantities using the previous estimates $\hat{x}_{k|k}$ and the mean voltage vector $\langle u_{k-1} \rangle$ actually applied to the system in the period $t_{k-1}$ to $t_k$. The second step corrects the predicted state estimate and covariance matrix by the measured actual motor phase currents.

*Step 1: Prediction (time update)*

$$\hat{x}_{k|k-1} = F_d\big(\hat{x}_{k-1|k-1}\big)\hat{x}_{k-1|k-1} + G_d\langle \boldsymbol{u}_{k-1} \rangle \tag{29}$$

$$P_{k|k} = \Phi_{dk-1} P_{k-1|k-1} \Phi_{k-1}^{'} + Q_d \tag{30}$$

*Step 2: Innovation (measurement update)*

$$\hat{x}_{k|k} = \hat{x}_{k|k-1} + K_k\big(y_k - H\hat{x}_{k|k-1}\big) \tag{31}$$

$$P_{k|k} = P_{k|k-1} - K_k H P_{k|k-1} \tag{32}$$

The Kalman gain is calculated by:

$$K_k = P_{k|k-1} H^{'} \big[H P_{k|k-1} H + R_d\big]^{-1} \tag{33}$$

The covariance update involves subtraction and thus can result in loss of symmetry and positive definiteness due to rounding errors. Joseph's form covariance update [14] avoids this at the expense of some computational burden:

$$\begin{aligned} P_{k|k} = [I - K_k H_{k-1}] P_{k|k-1} [I - K_k H_{k-1}]^{-1} \\ + K_k R_d K_k^{'} \end{aligned} \tag{34}$$

## 6.3 UKF algorithm

The UKF is a derivative free alternative to the EKF [14]. The basic mechanism for UKF is the same as the one described above by the equations (29) and (31). The difference is that the UKF performs the state estimation *by approximating the probability distribution after performing the computation using the nonlinear function*, rather than approximating the nonlinearity itself as in the EKF. To do this, the UKF utilizes the *Unscented Transformation* (UT).

A set of deterministic sample points is taken around the last known state and propagated through the real nonlinear function. With these results, a mean and covariance can be approximated using a weighted sample mean and covariance of the transferred sample points. These weighted sample points are generated as follows. Consider the state variable **x** with dimension $L$ having mean $\hat{x}$ and covariance $P_x$. We now choose a set of $2L$ +1 weighted samples $\chi_i$ (sigma points) deterministically so that they completely represent the true mean and covariance of state **x**.

$$\begin{aligned} \chi_0 &= \hat{x} \\ \chi_i &= \hat{x} + \left(\sqrt{(L+\lambda)P_x}\right)_i, i = 1, \dots, L \\ \chi_i &= \hat{x} - \left(\sqrt{(L+\lambda)P_x}\right)_i, i = n+1, \dots, L \\ W_0^{(m)} &= \lambda/(L+\lambda) \\ W_0^{(c)} &= W_0^{(m)} + 1 - \alpha^2 + \beta \\ W_i^{(m)} &= 1/2(L+\lambda) \end{aligned} \tag{35, 36}$$

Where $\lambda = \alpha^2(L+K) - L$ indicates a scaling parameter. The superscripts *m*, *c*, denote the weight point for mean or covariance calculation, respectively. The constant $\alpha$ determines the spread of the sigma points around **x**, and is set to a small positive value (e.g., $1 \le \alpha \le 10^{-4}$). The constant $\kappa$ is a secondary scaling parameter which is usually set to (3−*L*), and $\beta$ is used to include prior knowledge of the distribution of **x** (for Gaussian distribution $\beta = 2$ is optimal). $\left(\sqrt{(L+\lambda)P_x}\right)_i$ is the *i*-th row or column of the matrix square root of $(L+\lambda)P_x$ , and $W_i$ is the weight associated with the *i*-th sigma point so that $\sum_{i=0}^{2L} W_i = 1$. Now each point is propagated through the nonlinear function to yield a set of transformed sigma points.

$$Y_i = g(X_i) \tag{37}$$

The mean and covariance of **y** are approximated by the weighted average mean and covariance of the transformed sigma points.

Tab. 4: UKF algorithm

Initialize the state mean and covariance
for k=1, ..., ∞
1. Calculate the sigma points using equations (35)(36)
2. Predict (time update):

$$x_{k|k-1} = \boldsymbol{F}\left[x_{k|k-1}, u_{k|k-1}\right]$$

$$\hat{x}_k^- = \sum_{i=0}^{2L} W_i^{(m)} X_{i,k|k-1}$$

$$P_k^- = \sum_{i=0}^{2L} W_i^{(c)}\left[X_{i,k|k-1} - \hat{x}_k^-\right]\left[X_{i,k|k-1} - \hat{x}_k^-\right]^T + Q$$

3. Correct (measurement update):

$$Y_{k|k-1} = \boldsymbol{H}\left[x_{k|k-1}\right]$$

$$\hat{y}_k^- = \sum_{i=0}^{2L} \mathrm{W}_i^{(m)} \mathrm{Y}_{i,k|k-1}$$

$$P_{y_k y_k} = \sum_{i=0}^{2L} W_i^{(c)}\left[Y_{i,k|k-1} - \hat{y}_k^-\right]\left[Y_{i,k|k-1} - \hat{y}_k^-\right]^T + R$$

$$P_{x_k y_k} = \sum_{i=0}^{2L} W_i^{(c)}\left[X_{i,k|k-1} - \hat{x}_k^-\right]\left[Y_{i,k|k-1} - \hat{y}_k^-\right]^T$$

$$K_k = P_{x_k y_k} P_{y_k y_k}^{-1}$$

$$\hat{x}_k = \hat{x}_k^- + K_k(\hat{y}_k - \hat{y}_k^-)$$

$$P_k^- = P_k^- - K_k P_{y_k y_k} K_k^T$$

Table 4 shows the standard UKF algorithm for the additive (zero mean) case which is used for the simulations.

$$\hat{y} = \sum_{i=0}^{2L} W_i Y_i \tag{38}$$

$$P_y = \sum_{i=0}^{2L} W_i (Y_i - \hat{y})(Y_i - \hat{y})^T \tag{39}$$

## 7 SIMULATION RESULTS

To verify the state estimation performance of the UKF and the EKF on a AF PMSM, a number of simulations were carried out for different operating conditions. The EKF and UKF algorithms were implemented in SIMULINK environment. The parameters of the motor model and simulation are as following:

Stator winding self inductance $L_s = 32mH$, Stator winding resistance $R_s = 5\Omega$ , Back EMF constant $K_e = 0.215\, Vs/Rad$, Damping $B = 0.001$ Ns/rad , Number of Pole-Pairs $P = 2$ , Rotor Inertia $J = 0.6 \times 10^{-3} Kg.m^2$ , Nominal speed $\omega_n = 190\, Rad/Sec$ , Nominal Torque $T_n = 2N.m$ , Drive current limit $I_{max} = 16A$ , Drive voltage limit $V_{max} = 200V$, $\alpha = 1$ , $\beta = 2$ , $K = 0$

At first, starting and speed reversal performance of the sensor-less drive were compared. For this purpose, a SIMULINK model was developed as demonstrated in Fig. 5. Motor starts with nominal speed 1800 rpm in no-load condition. At *t=0.1s* speed reversal command is applied. Fig. 6 illustrates that the motor drive tracks speed command well. In this simulation, a noise with *0.5 A* was added to the current measurements to test the robustness of the system against noise corruption. Fig. 7 shows the resulting speed and position estimation performances. A set of further simulations was carried out to evaluate loading and un-loading performances of the system. Drive system starts in no-load condition and then a nominal load is applied to motor after *0.1s*. Afterwards, motor is un-loaded at *t=0.2s* and then speed is reversed at *t=0.3s.* A nominal step load applied to the motor at *t=0.4s* and at the end the motor is un-loaded. The obtained results have been illustrated in Fig. 8. And shows that the speed estimation performance of the filters subsequent to the introduced step load changes. The simulation results clearly indicate that both filters give good performances under loading and un-loading conditions. Nevertheless, the motor speed exhibits more oscillations but with the UKF during the transient period before settling to the steady state. However, it has smoother steady state characteristic compared with the EKF. For the considered drive system, the transient periods for the UKF and EKF are *0.05 s* and *0.03 s*, respectively. Fig. 9 shows the comparison between speed and position estimation errors in UKF and EKF algorithms.

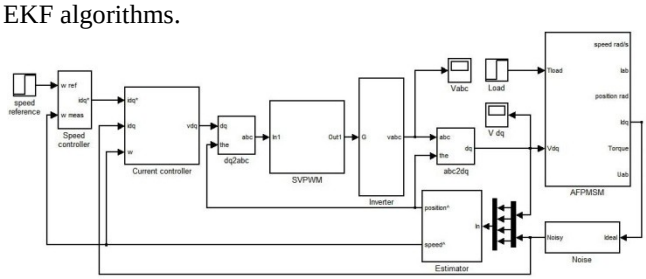

Fig. 5: Sensor-less control block diagram

### 7.1 Comparison

To compare the state estimation of the EKF and UKF in more detail, the estimation errors are squared and accumulated during the simulation run. The results are shown in Fig. 10 for the no-load and full speed four-quadrant simulation cases shown in Figs. 7 and 9. It can be observed that the EKF performs slightly better than UKF during no-load startup. During the speed reversal, however, the UKF performs better, resulting in a much lower accumulated error count. Both estimators give good steady-state performance. After a transient period, the estimation error tends to zero, as observed in Fig. 7. The transient response of the EKF seems slightly better and the steady-state condition is reached in a shorter time. It can be observed that the speed estimate of the UKF is less noisy than that of the EKF as indicated by the thinner speed error trace. As observed in Fig. 10, speed reversal performance of UKF is slightly better than EKF but the steady-state performance of UKF is significantly better than EKF. The dynamic response of the EKF, however, is better in no-load condition as can be seen from Figs. 7 and 10. But, UKF performs better in full load condition.

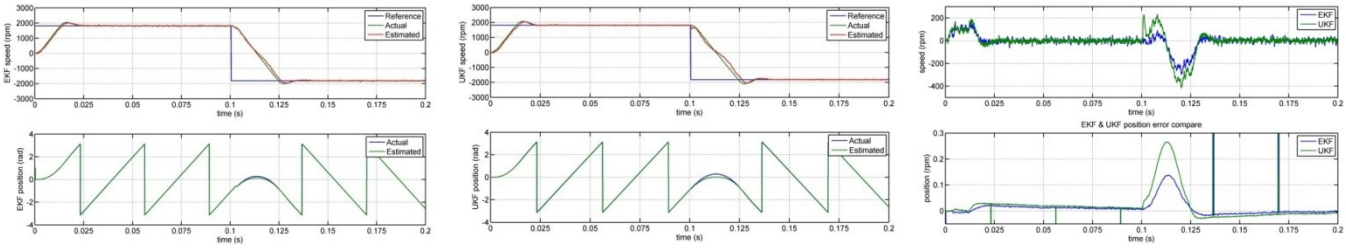


Fig. 6: EKF & UKF speed reversal performance

Fig. 7: EKF & UKF speed reversal test scenario

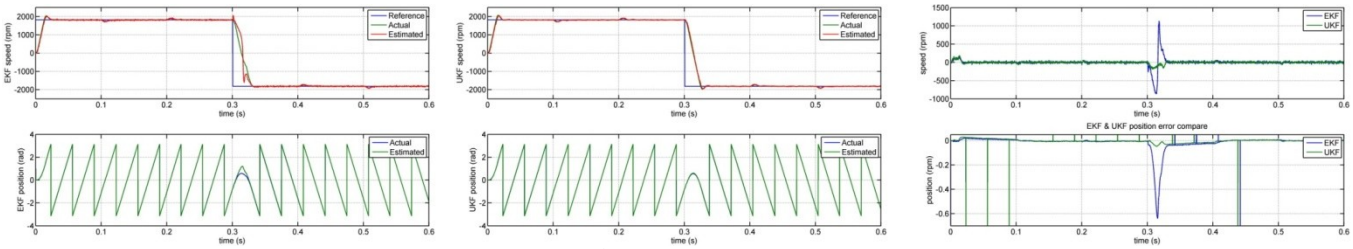


Fig. 8: EKF & UKF loading & un-loading performance

Fig. 9: EKF & UKF loading & un-loading error

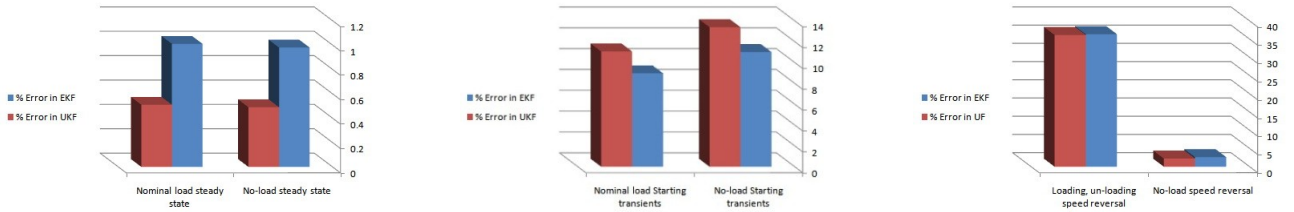


Fig. 10: EKF & UKF loading & un-loading error

## 8 CONCLUSION

An IMC-based current controller has been implemented for a sensor-less AFPMSM drive system using the SVPWM technique. The EKF and UKF estimation algorithms have been comparatively developed and evaluated for such a control system in a MATLAB software package environment. Both estimators are found to be suitable candidates for sensor-less control of AFPMSM drives. The EKF performs slightly better during motor start-up, but the UKF performs better in tracking the speed. Nevertheless, for industrial applications where steady state performance is critical, there is no clear preference for either estimation filter. It is observed that the UKF seems more promising under noisy conditions with better filter characteristics than the EKF.

## REFERENCES


[1] S. Ogasawara, M. Nishimura, H. Akagi, A. Nabae, and Y. Nakanishi, “A high performance AC servo system with permanent magnet synchronous motors,” IEEE Transactions on Industrial Electronics, vol. 33, no. 1, pp. 87-91, 1986.

[2] Zheng-Guang Wang, Jian-Xun Jin, You-Guang Guo, and Jian-Guo Zhu “SVPWM Techniques and Applications in HTS PMSM Machines” Control journal of electronic science and technology of china, VOL. 6, NO. 2, JUNE 2008

[3] B. T. Ooi, J. C. Salmon, J. W. Dixon, and A. B. Kulkarni, “A three phase controlled-current PWM converter with leading power factor,” IEEE Transactions on Ind. Application, vol. 23, no. 1, pp. 78-84, 1987

[4] J. W. Dixon and B. T. Ooi, “Indirect current control of a unity power factor sinusoidal current boost type three-phase rectifier,” IEEE Transactions on Ind. Electron, vol. 35, no. 4, pp. 508-515, Nov. 1988.

[5] P. Pillay and R. Krishnan, "Modeling of permanent magnet motor drives," IEEE Trans. Industrial Electronics, vol 35 , no. 4 , Nov. 1988, pp.537-541.

[6] S. M. Hosseini, M. Agha-Mirsalim, and M. Mirzaei, “Design, prototyping, and analysis of low cost axial-flux coreless permanent-magnet generator,” IEEE Trans. Magn., vol. 44, no. 1, pp. 75–80, Jan. 2008.

[7] J. A. Tapia, D. González, R. Wallace, and A. Valenzuela, “Axial flux surface mounted PM machine with field weakening capability,” in Int.Conf. Electrical Machines, ICEM’2004, Krakow, Poland.

[8] R. Krishnan and A. J. Beutler, “Performance and design of an axial field permanent magnet synchronous motor servo drive,” in Proc. IEEE IAS Annu. Meeting, pp. 634-640, 1985.

[9] D. G. Holmes and T. A. Lipo, Pulse Width Modulation for Power Converters—Principle and Practice, IEEE Press/Wiley-Interscience, New York, 2003.

[10] M. H. Rashid, Power Electronics Handbook, Academic Press, New York, 2001.

[11] Lennart Harnefors, Hans-Peter Nee, “Model-Based Current Control of AC Machines Using the Internal Model Control Method” IEEE transaction on industry application, VOL. 34, NO. 1, Jan / Feb 1998

[12] S. Bolognani, L. Tubiana, M. Zigliotto, “EKF-based sensorless IPM synchronous motor drive for flux-weakening applications,” IEEE Trans. Industry Applications, vol. 39, no. 3 , May-June 2003, pp. 768–775.

[13] R. Dhaouadi, N. Mohan and L. Norum, “Design and implementation of an extended Kalman filter for the state estimation of a permanent magnet synchronous motor,” IEEE Trans. Power Electronics, vol. 6, no. 3 , July 1991, pp. 491–497.

[14] Simon Haykin, Kalman Filtering and neural networks. Communications Research Laboratory, McMaster University, Hamilton, Ontario, Canada, John Wiley & Sons, Inc. New York, ISBN 0-471-36998-5.

[15] Gene F. Franklin, J. David Powell and Michael Workman, Digital Control of dynamic systems. Addison Wesley Longman, Inc., 1998, ISBN 0-201-82054-44.

[16] Frank L. Lewis, Applied Optimal Control & estimation: digital design & implementation. Prentice-Hall, Inc., 1992, ISBN 0-13-040361-x.